Chapter 3 Shapes of Unsymmetric Composite Plates

3.1 Chapter Outline

As is well known, unsymmetric laminates exhibit bending-stretching elastic coupling, a characteristic that perhaps can be used to advantage for elastic tailoring. However, unsymmetric laminates that are cured at an elevated temperature deform severely as they are cooled to their service temperature. These deformations may be large enough to render an unsymmetrically laminated structural component unsuited for its intended usage. Here models are developed to predict the deformations associated with cooling an unsymmetric laminate from the autoclave cure temperature to a service temperature, say, room temperature. The analyses consist of finite-element methods and the Rayleigh-Ritz total potential energy minimization technique. The Rayleigh-Ritz method will be considered because it is an efficient way to conduct an analysis and can offer more physical insight into the problem than a finite-element analysis. The finite-element models will be used to compare with and supplement the Rayleigh-Ritz models. Interest centers on square unsymmetric composite panels that exhibit strong elastic couplings. Figure 3.1 shows the geometry of the eight-layer panels under consideration. The influence of the side length L on the cooled shape is considered, though there is specific interest in 12 in. by 12 in. panel (L=12 in.). A total of seven laminates will be investigated. These laminates are divided into cross-ply laminates and angle-ply laminates. Both classes of laminates are unsymmetric, however, the cross-ply laminates do not contain any layers with off-axis orientations. This characterization leads to a simplification of the analyses. Therefore, Section 3.2 will be devoted to the study of cross-ply laminates, while Section 3.3 will be devoted to the study of angle-ply laminates. The models developed will be used to predict the deformations of the laminates due to a temperature change of -280°F. The results of manufacturing and measuring the cure induced deformations of a number of laminates will be presented and compared with predictions.

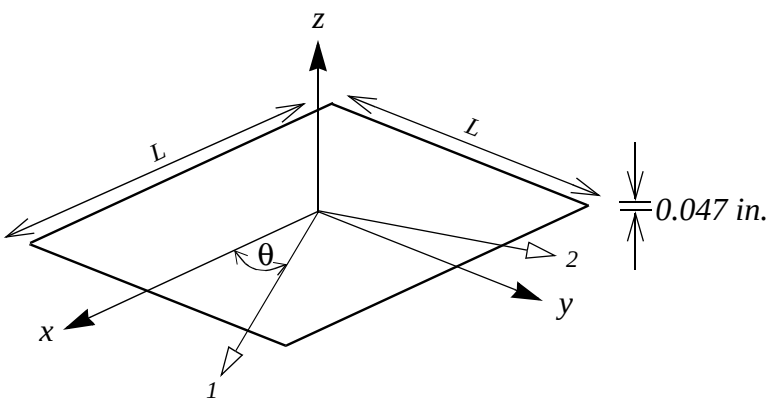

Fig. 3.1 Panel geometry and coordinate system

Figure 3.2 depicts the problem statement as a four-step manufacturing process. The first step in the process is the lay-up of pre-impregnated composite layers upon the tool. The tool has specific dimensions, in this case a flat surface. This step is accomplished in a room temperature environment. The second step is the elevated temperature curing of the composite in an autoclave. Step three, cooling to room temperature, is when many of the effects of the lack of laminate symmetry become evident. The temperature decrease from the stress free curing temperature to room temperature, coupled with the unsymmetric laminate construction, causes the shape and dimensions of the plate to be different than those of the uncured plate and tool. The objective of this section is to develop models to predict the cooled shapes of these laminates.

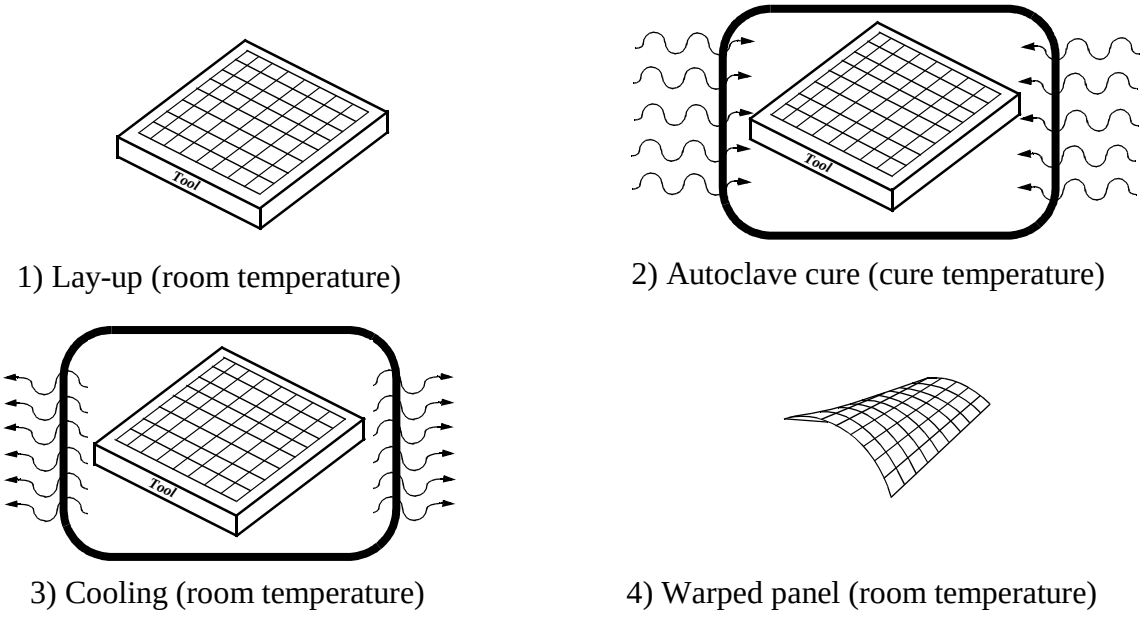

Fig. 3.2 Problem statement

3.2 Cross-ply Laminates

This section will focus on the deformation of cross-ply laminates. Table 3.1 shows the construction of the four cross-ply laminates that will be considered.

Table 3.1 Cross-ply laminate construction

Laminate	**Layup**
Cross-ply 1	$[0_4/90_4]_T$
Cross-ply 2	$[0_6/90_2]_T$
Cross-ply 3	$[0_4/90_2/0_2]_T$
Cross-ply 4	$[0_2/90_2/0_2/90_2]_T$

These cross-ply laminates are highly unsymmetric, resulting in large deformations that can only be accurately modeled using geometrically nonlinear kinematic theories. Therefore, three geometrically nonlinear models will be developed.

3.2.1 The Rayleigh-Ritz Models

The Rayleigh-Ritz approach utilizes the minimization of the total potential energy to find approximate solutions. Initially, a four-term displacement field approximation was developed based upon previous work by Hyer [5]. In this work, the reference surface displacements were approximated as

$$u^o(x,y) = cx - \frac{a^2x^3}{6} - \frac{abxy^2}{4} \tag{3.1}$$

$$v^o(x,y) = dy - \frac{b^2y^3}{6} - \frac{abx^2y}{4} \tag{3.2}$$

$$w^o(x,y) = \frac{1}{2}(ax^2 + by^2) \tag{3.3}$$

The displacement field approximation is based on the observed deformations of cross-ply laminates. The constants *a, b, c,* and *d,* are to be determined through the minimization of total potential energy. These four constants make up the four-term Rayleigh-Ritz model. Due to the limited number of unknown coefficients, this displacement field based model is limited to predicting the deformations of cross-ply laminates. The assumed displacement fields are substituted into the von Kármán geometrically nonlinear kinematic relationships to compute the reference surface strains as

$$\begin{aligned} \epsilon_x^o &= \frac{\partial u^o}{\partial x} + \frac{1}{2}\beta_x^{o2} \\ \epsilon_y^o &= \frac{\partial v^o}{\partial y} + \frac{1}{2}\beta_y^{o2} \\ \gamma_{xy}^o &= \frac{1}{2}\left(\frac{\partial u^o}{\partial y} + \frac{\partial v^o}{\partial x}\right) + \beta_x^o\beta_y^o \end{aligned} \tag{3.4}$$

where,

$$\beta_x^o = -\frac{\partial w^o}{\partial x} \text{ and } \beta_y^o = -\frac{\partial w^o}{\partial y} \tag{3.5}$$

and reference surface curvatures as

$$\begin{aligned} \kappa_x^o &= \frac{\partial \beta_x^o}{\partial x} = -\frac{\partial^2 w^o}{\partial x^2} \\ \kappa_y^o &= \frac{\partial \beta_y^o}{\partial y} = -\frac{\partial^2 w^o}{\partial y^2} \\ \kappa_{xy}^o &= \frac{\partial \beta_x^o}{\partial y} + \frac{\partial \beta_y^o}{\partial x} = -2\frac{\partial^2 w^o}{\partial x \partial y} \end{aligned} \tag{3.6}$$

Using equations 3.1-3.3 in equations 3.5 and 3.6 results in the following expression for the reference surface strains:

$$\begin{aligned} \epsilon_x^o &= c - \frac{1}{4}aby^2 \\ \epsilon_y^o &= d - \frac{1}{4}abx^2 \\ \gamma_{xy}^o &= 0 \end{aligned} \tag{3.7}$$

The reference surface curvatures are given by

$$\begin{aligned} \kappa_x^o &= -a \\ \kappa_y^o &= -b \\ \kappa_{xy}^o &= 0 \end{aligned} \tag{3.8}$$

As can be seen for the cross-ply laminates, the twist curvature is assumed to be zero. It is also possible to approximate the reference surface strains and curvatures directly using a polynomial expression constructed of unknown constants. Dano and Hyer [6] utilized a 28-term approximation of reference surface strains to develop solutions for general unsymmetric laminates. They concluded that 14 of the 28 constants chosen to represent the strains and curvatures were negligible with respect to the remaining half. Therefore, a 14-term Rayleigh-Ritz model was developed here to supplement the four-term model and predict deformations of angle-ply laminates being considered in the next section. In the 14-term model the reference surface strains are expressed as

$$\epsilon_x^o(x,y) = a_0 + a_1x^2 + a_2xy + a_3y^2 \tag{3.9}$$

$$\epsilon_y^o(x,y) = b_0 + b_1x^2 + b_2xy + b_3y^2 \tag{3.10}$$

and

$$\gamma^o_{xy}(x,y) = 2c_0 + (c_1c_2 - \frac{c_3^2}{4} + 2a_3 + 2b_1)xy + (\frac{1}{2}(\frac{c_1c_3}{2} + a_2) + c_4)x^2 + (\frac{1}{2}(\frac{c_2c_3}{2} + b_2) + c_5)y^2 \tag{3.11}$$

The out-of-plane displacement field is expressed as

$$w^o(x,y) = \frac{1}{2}(c_1x^2 + c_2y^2 + c_3xy) \tag{3.12}$$

The curvatures can then be directly computed from the kinematic relationships of equation 3.6 as

$$\begin{aligned} \kappa^o_x &= -c_1 \\ \kappa^o_y &= -c_2 \\ \kappa^o_{xy} &= -c_3 \end{aligned} \tag{3.13}$$

As can be seen, to accommodate more general laminates, a twist curvature is included. Invoking the plane-stress assumption by assuming all components of stress in the thickness direction are zero, the total potential energy may be rewritten as

$$\Pi = \frac{1}{2}\int_{-\frac{L_x}{2}}^{+\frac{L_x}{2}}\int_{-\frac{L_y}{2}}^{+\frac{L_y}{2}}\int_{-\frac{H}{2}}^{+\frac{H}{2}}((\sigma_x - \sigma_x^T)\epsilon_x + (\sigma_y - \sigma_y^T)\epsilon_y + (\tau_{xy} - \tau_{xy}^T)\gamma_{xy})dx\,dy\,dz \tag{3.14}$$

By assuming that the Kirchhoff hypothesis applies, the strains may be expressed in terms of reference surface strains and curvatures by

$$\begin{aligned} \epsilon_x &= \epsilon^o_x + z\kappa^o_x \\ \epsilon_y &= \epsilon^o_y + z\kappa^o_y \\ \gamma_{xy} &= \gamma^o_{xy} + z\kappa^o_{xy} \end{aligned} \tag{3.15}$$

Due to the assumption of plane-stress, the stress components may be written as,

$$\begin{aligned} \sigma_x &= \bar{Q}_{11}(\epsilon_x - \alpha_x\Delta T) + \bar{Q}_{12}(\epsilon_y - \alpha_y\Delta T) + \bar{Q}_{16}(\gamma_{xy} - \alpha_{xy}\Delta T) \\ \sigma_y &= \bar{Q}_{12}(\epsilon_x - \alpha_x\Delta T) + \bar{Q}_{22}(\epsilon_y - \alpha_y\Delta T) + \bar{Q}_{26}(\gamma_{xy} - \alpha_{xy}\Delta T) \\ \tau_{xy} &= \bar{Q}_{16}(\epsilon_x - \alpha_x\Delta T) + \bar{Q}_{26}(\epsilon_y - \alpha_y\Delta T) + \bar{Q}_{66}(\gamma_{xy} - \alpha_{xy}\Delta T) \end{aligned} \tag{3.16}$$

or

$$\begin{aligned} \sigma_x &= \bar{Q}_{11}\epsilon_x + \bar{Q}_{12}\epsilon_y + \bar{Q}_{16}\gamma_{xy} - \sigma_x^T \\ \sigma_x &= \bar{Q}_{12}\epsilon_x + \bar{Q}_{22}\epsilon_y + \bar{Q}_{26}\gamma_{xy} - \sigma_y^T \\ \tau_{xy} &= \bar{Q}_{16}\epsilon_x + \bar{Q}_{26}\epsilon_y + \bar{Q}_{66}\gamma_{xy} - \tau_{xy}^T \end{aligned} \tag{3.17}$$

where

$$\begin{aligned} \sigma_x^T &= (\bar{Q}_{11}\alpha_x + \bar{Q}_{12}\alpha_y + \bar{Q}_{16}\alpha_{xy})\Delta T \\ \sigma_y^T &= (\bar{Q}_{12}\alpha_x + \bar{Q}_{22}\alpha_y + \bar{Q}_{26}\alpha_{xy})\Delta T \\ \tau_{xy}^T &= (\bar{Q}_{16}\alpha_x + \bar{Q}_{26}\alpha_y + \bar{Q}_{66}\alpha_{xy})\Delta T \end{aligned} \tag{3.18}$$

and where the $\overline{Q}$'s are reduced stiffnesses and the α's are coefficients of thermal expansion. Equations 3.19 and 3.20 can be used to rewrite the total potential energy as

$$\Pi = \frac{1}{2}\int_{-\frac{L_x}{2}}^{+\frac{L_x}{2}}\int_{-\frac{L_y}{2}}^{+\frac{L_y}{2}}\int_{-\frac{H}{2}}^{+\frac{H}{2}} \Big\{(\sigma_x - \sigma_x^T)(\epsilon_x^o + z\kappa_x^o) + (\sigma_y - \sigma_y^T)(\epsilon_y^o + z\kappa_y^o) + (\tau_{xy} - \tau_{xy}^T)(\gamma_{xy}^o + z\kappa_{xy}^o)\Big\}\, dx\, dy\, dz \tag{3.19}$$

Carrying out the first integration through-the-thickness leads to,

$$\begin{aligned} \Pi &= \frac{1}{2}\int_{-\frac{L_x}{2}}^{+\frac{L_x}{2}}\int_{-\frac{L_y}{2}}^{+\frac{L_y}{2}} \Big\{(N_x - \hat{N}_x^T\Delta T)\epsilon_x^o + (N_y - \hat{N}_y^T\Delta T)\epsilon_y^o + (N_{xy} - \hat{N}_{xy}^T\Delta T)\gamma_{xy}^o \\ &+ (M_x - \hat{M}_x^T\Delta T)\kappa_x^o + (M_y - \hat{M}_y^T\Delta T)\kappa_y^o + (M_{xy} - \hat{M}_{xy}^T\Delta T)\kappa_{xy}^o\Big\}\, dxdy \end{aligned} \tag{3.20}$$

where the force resultants, N_x, N_y, N_{xy}, and moment resultants, M_x, M_y, M_{xy}, are defined as

$$
\begin{aligned}
N_x &\equiv \int_{-\frac{H}{2}}^{+\frac{H}{2}} \sigma_x dz = A_{11}\epsilon_x^o + A_{12}\epsilon_y^o + A_{16}\gamma_{xy}^o + B_{11}\kappa_x^o + B_{12}\kappa_y^o + B_{16}\kappa_{xy}^o - \hat{N}_x^T \Delta T \\
N_y &\equiv \int_{-\frac{H}{2}}^{+\frac{H}{2}} \sigma_y dz = A_{12}\epsilon_x^o + A_{22}\epsilon_y^o + A_{26}\gamma_{xy}^o + B_{12}\kappa_x^o + B_{22}\kappa_y^o + B_{26}\kappa_{xy}^o - \hat{N}_y^T \Delta T \\
N_{xy} &\equiv \int_{-\frac{H}{2}}^{+\frac{H}{2}} \tau_{xy} dz = A_{16}\epsilon_x^o + A_{26}\epsilon_y^o + A_{66}\gamma_{xy}^o + B_{16}\kappa_x^o + B_{26}\kappa_y^o + B_{66}\kappa_{xy}^o - \hat{N}_{xy}^T \Delta T \\
M_x &\equiv \int_{-\frac{H}{2}}^{+\frac{H}{2}} z\sigma_x dz = B_{11}\epsilon_x^o + B_{12}\epsilon_y^o + B_{16}\gamma_{xy}^o + D_{11}\kappa_x^o + D_{12}\kappa_y^o + D_{16}\kappa_{xy}^o - \hat{M}_x^T \Delta T \\
M_y &\equiv \int_{-\frac{H}{2}}^{+\frac{H}{2}} z\sigma_y dz = B_{12}\epsilon_x^o + B_{22}\epsilon_y^o + B_{26}\gamma_{xy}^o + D_{12}\kappa_x^o + D_{22}\kappa_y^o + D_{26}\kappa_{xy}^o - \hat{M}_y^T \Delta T \\
M_{xy} &\equiv \int_{-\frac{H}{2}}^{+\frac{H}{2}} z\tau_{xy} dz = B_{16}\epsilon_x^o + B_{26}\epsilon_y^o + B_{66}\gamma_{xy}^o + D_{16}\kappa_x^o + D_{26}\kappa_y^o + D_{66}\kappa_{xy}^o - \hat{M}_{xy}^T \Delta T
\end{aligned}
\tag{3.21}
$$

and the thermal force and moment resultants are defined as

$$
\begin{aligned}
\hat{N}_x^T &\equiv \int_{-\frac{H}{2}}^{+\frac{H}{2}} \left(\bar{Q}_{11}\alpha_x + \bar{Q}_{12}\alpha_y + \bar{Q}_{16}\alpha_{xy}\right) dz \\
\hat{N}_y^T &\equiv \int_{-\frac{H}{2}}^{+\frac{H}{2}} \left(\bar{Q}_{12}\alpha_x + \bar{Q}_{22}\alpha_y + \bar{Q}_{26}\alpha_{xy}\right) dz \\
\hat{N}_{xy}^T &\equiv \int_{-\frac{H}{2}}^{+\frac{H}{2}} \left(\bar{Q}_{16}\alpha_x + \bar{Q}_{26}\alpha_y + \bar{Q}_{66}\alpha_{xy}\right) dz \\
\hat{M}_x^T &\equiv \int_{-\frac{H}{2}}^{+\frac{H}{2}} \left(\bar{Q}_{11}\alpha_x + \bar{Q}_{12}\alpha_y + \bar{Q}_{16}\alpha_{xy}\right) z dz \\
\hat{M}_y^T &\equiv \int_{-\frac{H}{2}}^{+\frac{H}{2}} \left(\bar{Q}_{12}\alpha_x + \bar{Q}_{22}\alpha_y + \bar{Q}_{26}\alpha_{xy}\right) z dz \\
\hat{M}_{xy}^T &\equiv \int_{-\frac{H}{2}}^{+\frac{H}{2}} \left(\bar{Q}_{16}\alpha_x + \bar{Q}_{26}\alpha_y + \bar{Q}_{66}\alpha_{xy}\right) z dz
\end{aligned}
\tag{3.22}
$$

The stresses defined in equations 3.16-3.18 can be used together with the strains to form the expression for the total potential energy, equation 3.20. The Rayleigh-Ritz method calls for the minimization of the total potential energy with respect to the unknown coefficients, leading to a set of algebraic equations which can be solved for the unknown coefficient to arrive at approximate solutions. Since these unsymmetric laminates may have multiple solutions, or more than one possible deformed shape, a stability analysis is performed to determine the stable shapes that are physically admissible. This is accomplished by computing the second variation of the total potential energy, which can be expressed as

$$\delta^2\Pi = \left[\begin{array}{cccc} \delta a & \delta b & \delta c & \delta d \end{array} \right] \left[C \right] \left[\begin{array}{c} \delta a \\ \delta b \\ \delta c \\ \delta d \end{array} \right] \tag{3.23}$$

The stability of a particular solution is investigated by examining the eigenvalues of the matrix [C]. Solutions that lead to all positive eigenvalues are stable.

3.2.2 Finite-Element Models

Finite-element models were developed based on the geometry of Fig. 3.1. The model consists of 2,116 S9R5 shear deformable shell elements made up of 8,663 nodes constituting 43,315 degrees of freedom. The eight-layer models utilizes 3 integration points per layer, for a total of 24 integration points through the thickness. These models were solved using the geometrically nonlinear large deformation theory in ABAQUS. This model differs from its Rayleigh-Ritz counterparts by allowing for transverse shear deformations.

3.2.3 Experimental Measurements

Actual specimens were constructed and measured to compare with predictions. The specimens were measured by a mechanical surface profilometer and data acquisition software. Due to the realities of the measurement process, the panels were not scanned all the way to the edges. This is the reason why the scanned panels will appear smaller when compared to the predictions in the following section.

3.2.4 Results

Due to its analytical efficiency, the four-term Rayleigh-Ritz model was used first to compute the curvatures as a function of panel size. Figures 3.3-3.6 show the panel curvatures as a function of side length for each of the four cross-ply laminates being considered. The figures show the curvatures of the specific side lengths investigated. The solid symbols represent stable solutions, while the open symbols represent unstable solutions. By examining the relationship between the curvature and the side length, it can be seen that the four panels under consideration have multiple room temperature shapes after a certain side length has been exceeded. However,

the panels being considered in the current work are 12 in. by 12 in. Therefore, a dotted vertical line has been added to the figures to indicate the side length of the actual panels being considered. By comparing results at this side length, it can be seen that two of the four laminates have multiple room-temperature shapes. The $[0_4/90_4]_T$ laminate has multiple room-temperature shapes, while the $[0_6/90_2]_T$ laminate has only one shape at this side length. The $[0_4/90_2/0_2]_T$ laminate has only one shape at this side length, while the $[0_2/90_2/0_2/90_2]_T$ laminate has multiple shapes. The existence of two stable shapes means that one stable shape can be snapped into the other stable shape through the application of small moments along the edges. This unique behavior is one of the characteristics of unsymmetric panels cured at elevated temperature. The information regarding single or multiple shapes is very valuable in the development of the finite-element models. This is because the geometrically nonlinear solver in ABAQUS can not directly find the multiple shapes predicted by the Rayleigh-Ritz analysis. Each of the multiple shapes was found by ABAQUS after including slight geometric imperfections to bias the initial geometry towards the specific shape predicted by the Rayleigh-Ritz models. The slight imperfection starts the analysis along the solution path towards the predicted shape until the solver converges upon an equilibrium solution.

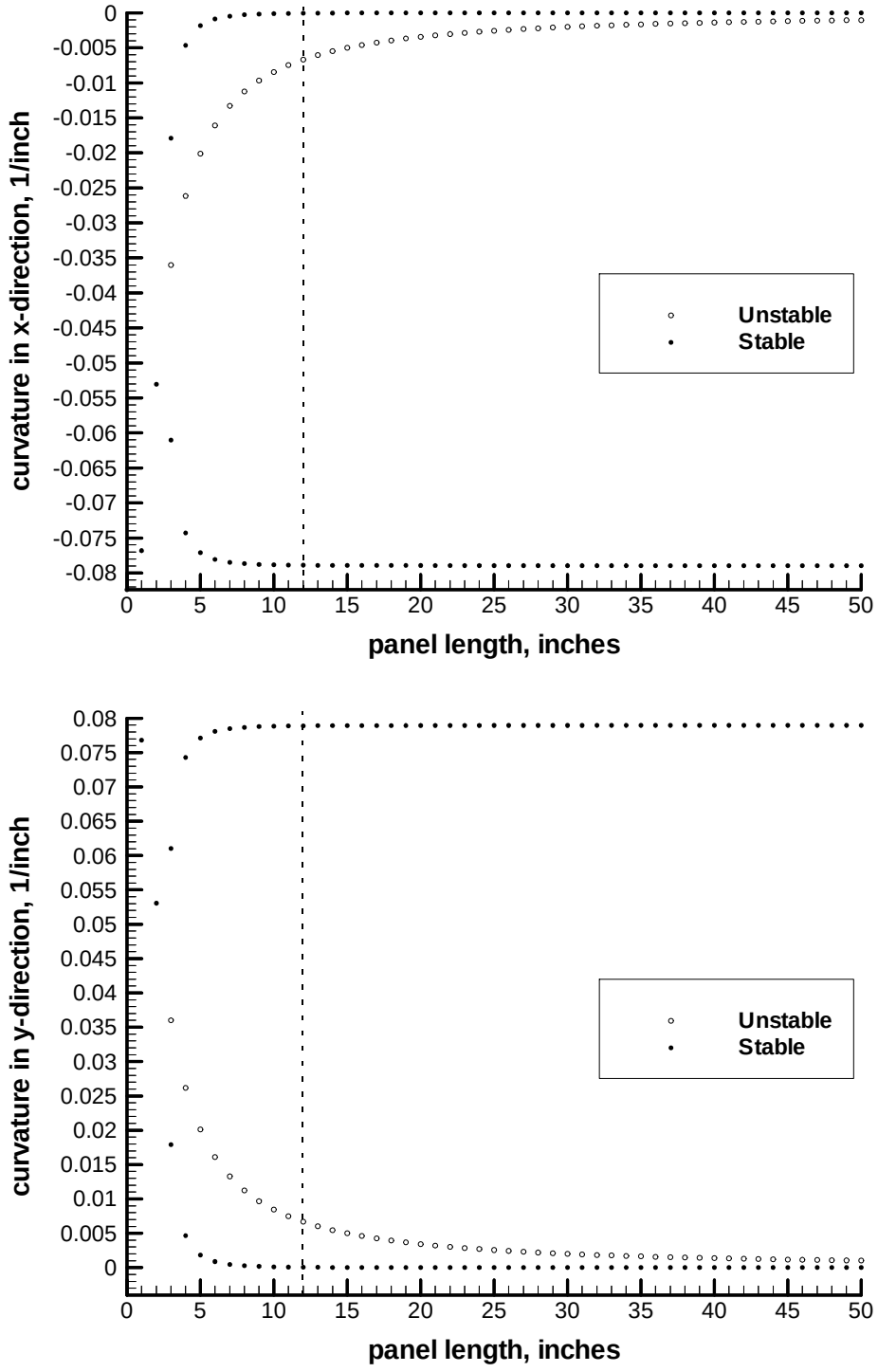

Fig. 3.3 Curvature vs. side length for $[0_4/90_4]_T$ laminate, ΔT=-280°F

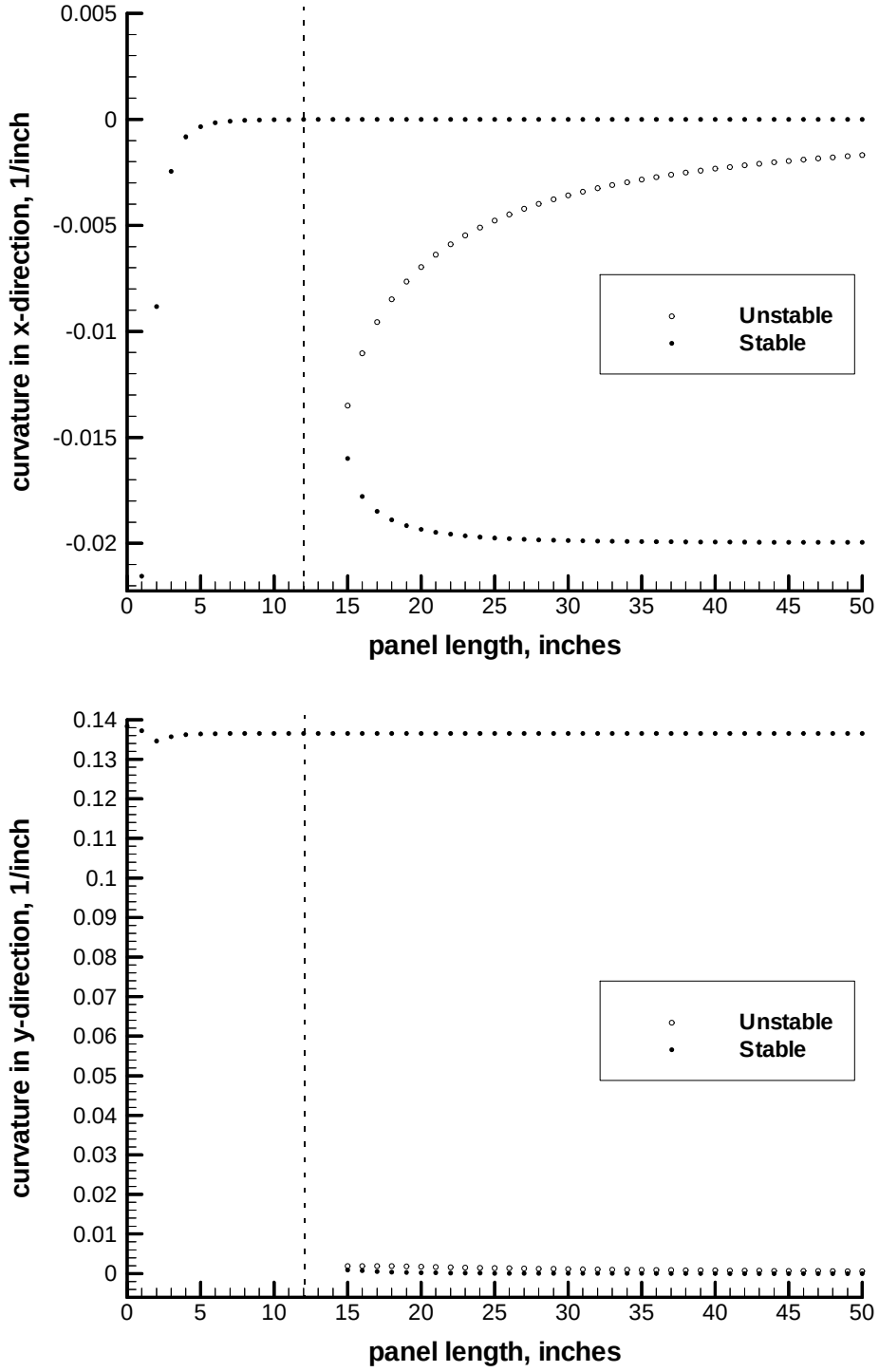

Fig. 3.4 Curvature vs. side length for $[0_6/90_2]_T$ laminate, ΔT=-280°F

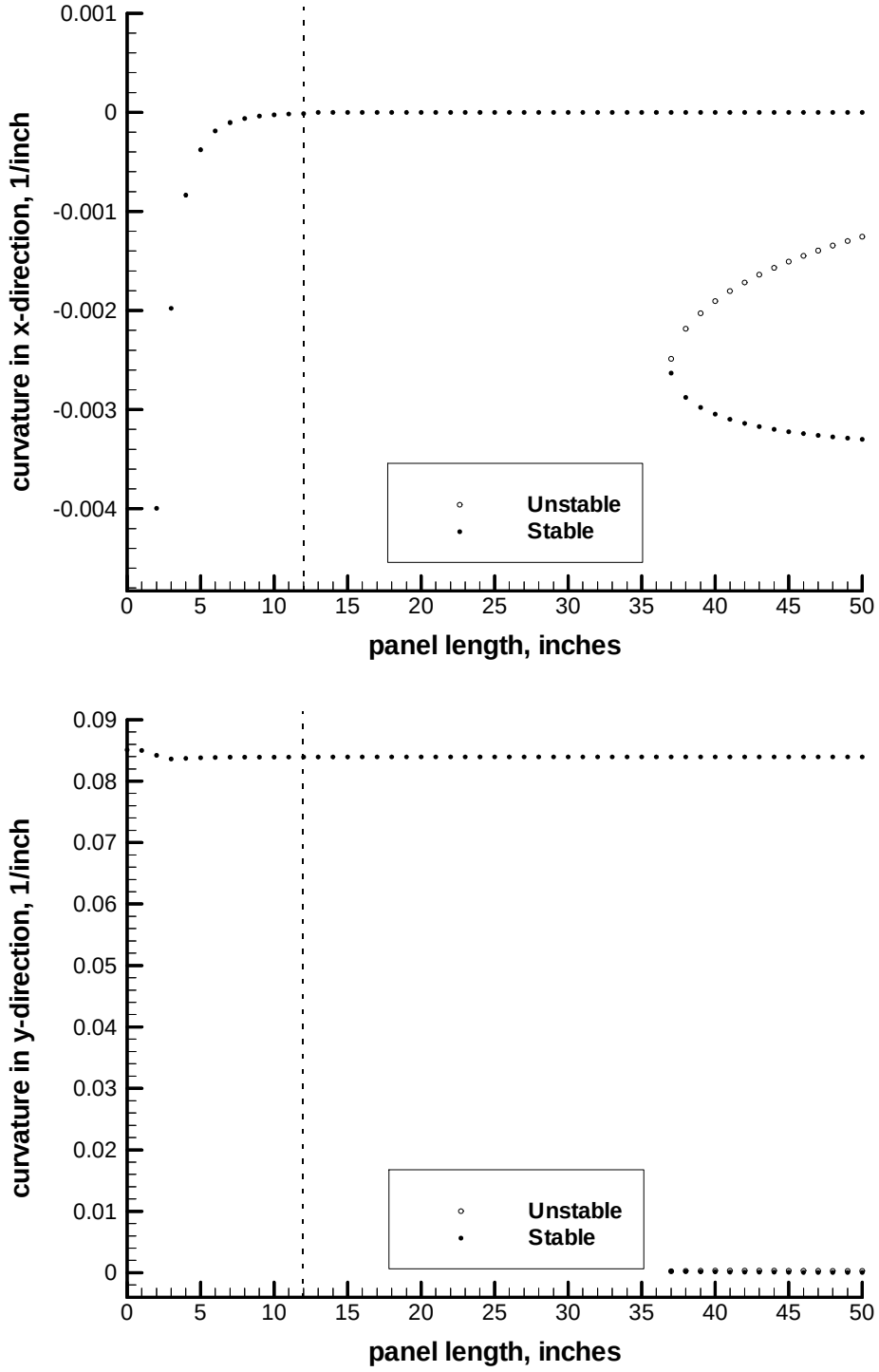

Fig. 3.5 Curvature vs. side length for $[0_4/90_2/0_2]_T$ laminate, ΔT=-280°F

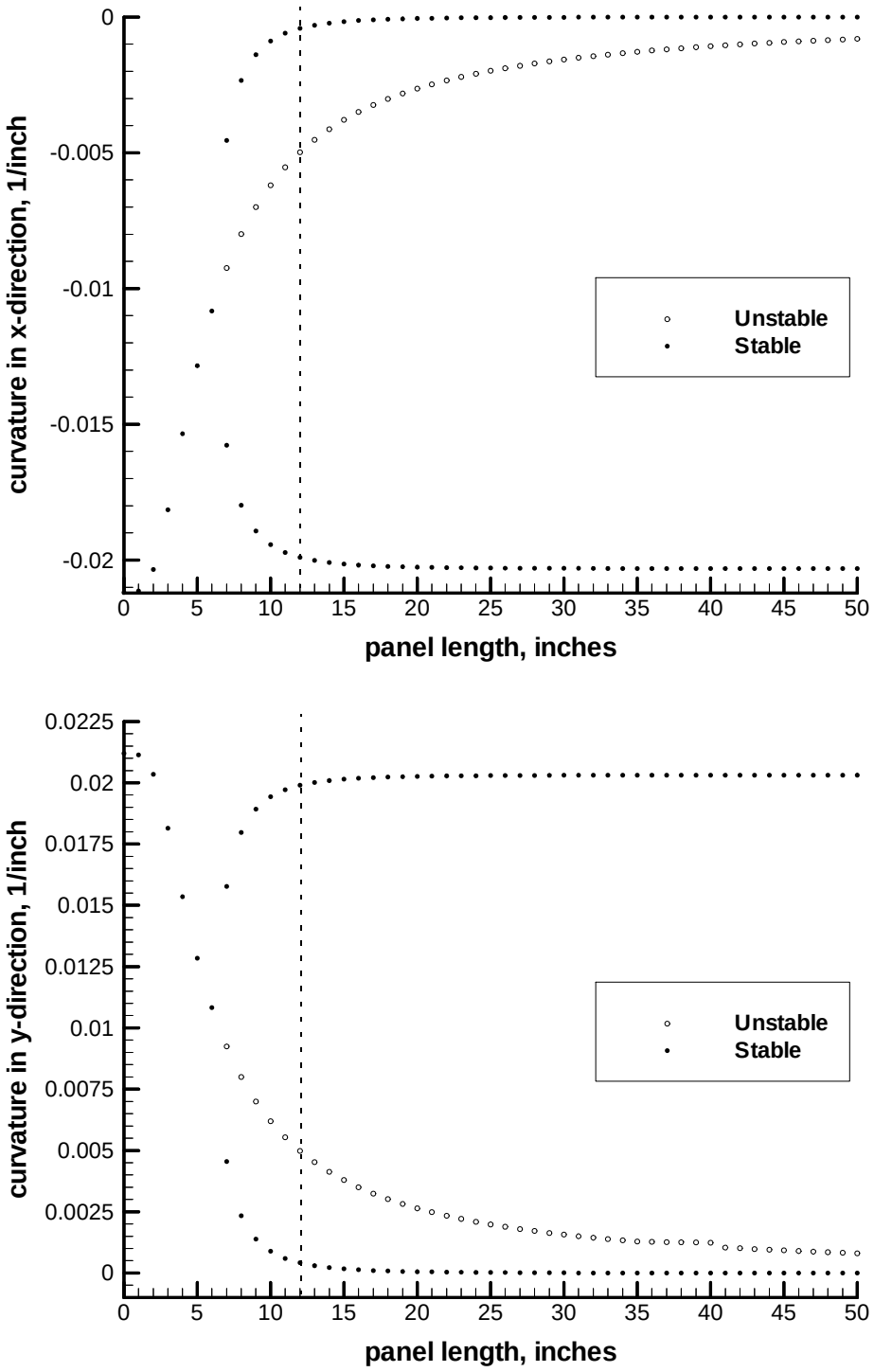

Fig. 3.6 Curvature vs. side length for $[0_2/90_2/0_2/90_2]_T$ laminate, ΔT=-280°F

Figure 3.7 shows one of the stable predicted shapes for a $[0_4/90_4]_T$ laminate at room temperature. Figure 3.7(a) shows the solution predicted by the four-term Rayleigh-Ritz model. Figure 3.7(b) shows the solution predicted by the 14-term Rayleigh-Ritz model. Figure 3.7(c) shows the solution predicted by the finite-element model. Figure 3.7(d) shows the deformed shape of the actual panel. The agreement between the three predictions and the experimental results is excellent. It should be noted that another stable shape exists for this laminate. The predicted alternate shapes are shown in Fig. 3.8. It is important to note the equal but opposite character of the two overall curvatures associated with the two shapes of the $[0_4/90_4]_T$ laminate.

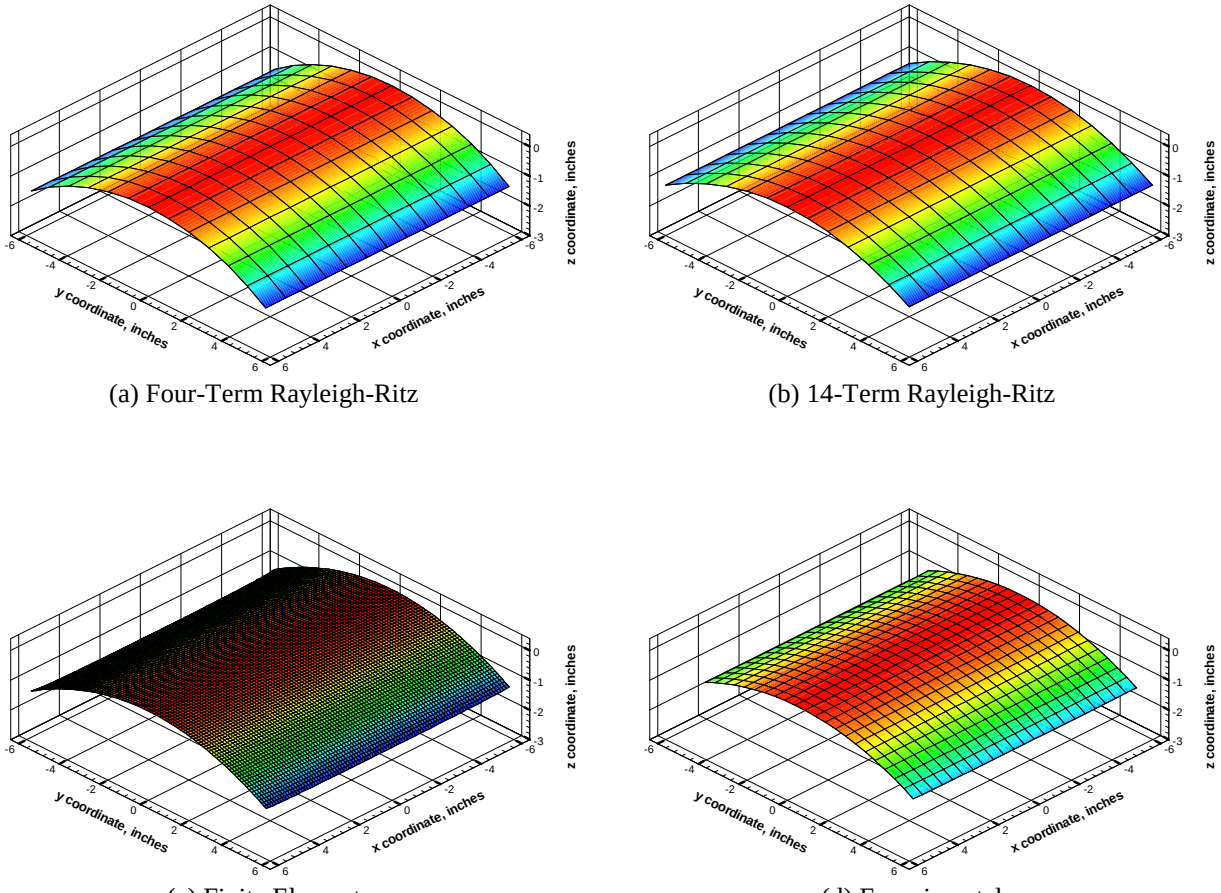

(a) Four-Term Rayleigh-Ritz

(b) 14-Term Rayleigh-Ritz

(c) Finite Element

(d) Experimental

Fig. 3.7 The primary stable shape of $[0_4/90_4]_T$ laminate, ΔT=-280°F

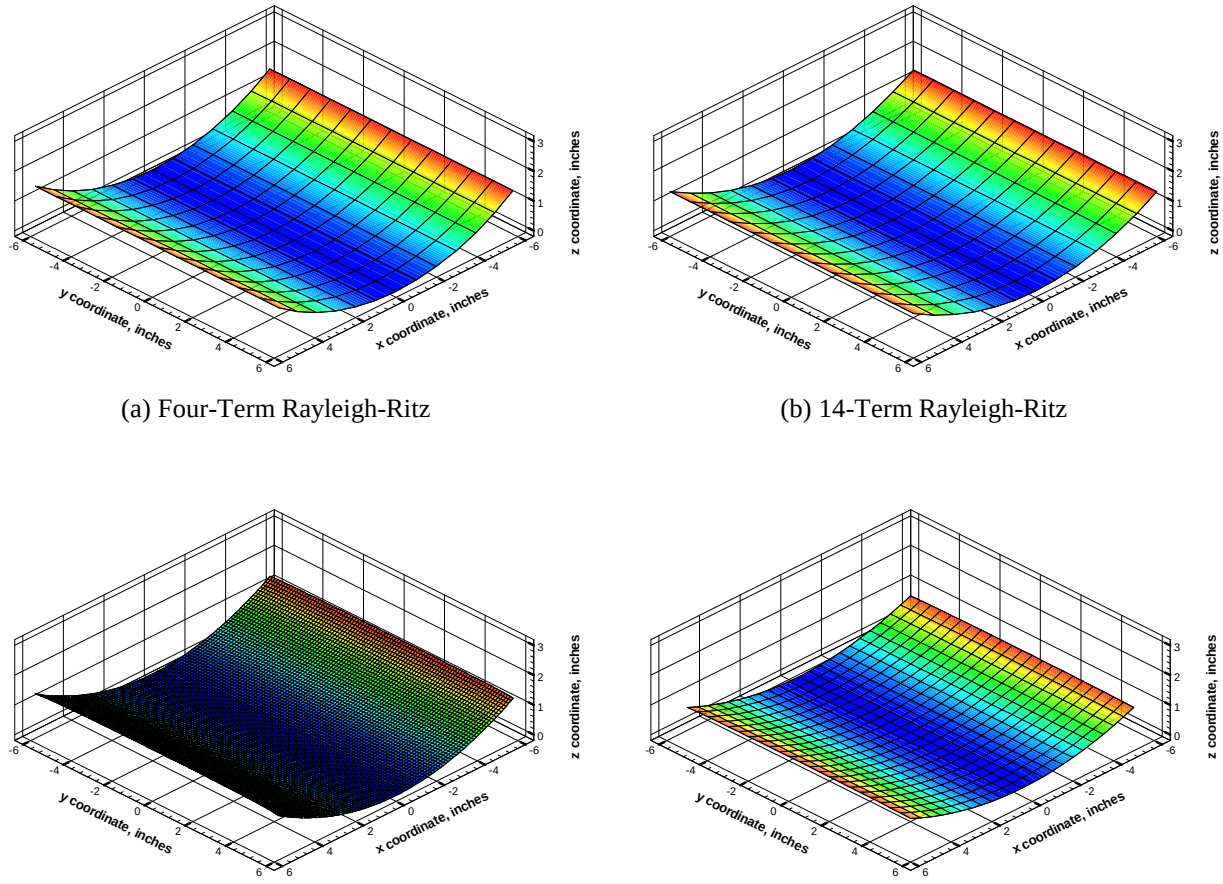

(a) Four-Term Rayleigh-Ritz

(b) 14-Term Rayleigh-Ritz

(c) Finite Element

(d) Experimental

Fig. 3.8 The alternate stable shape of $[0_4/90_4]_T$ laminate, ΔT=-280°F

Though the overall comparison of the three predictions shown in Figs. 3.7 and 3.8 is good, details of the differences among the three predictions of Fig. 3.7 may be readily observed in Fig. 3.9. The figure shows the normalized out-of-plane displacements along two edges of the laminate as predicted by the three models. The differences between the predictions are most visible in the top figure. This shows the variation of the *z*-displacements, normalized by the laminate thickness, with the *x*-coordinate along what appears to be the straight edge of the deformed panel. The four-term Rayleigh-Ritz model predicts the greatest edge displacements, and the displacement is almost constant along this edge, predicting very little curvature along the edge. The 14-term Rayleigh-

Ritz model predicts the least edge displacements, while predicting somewhat more curvature along the edge. The edge displacements predicted by the finite-element model are between those predicted by the two Rayleigh-Ritz models. However, it is important to note that the finite-element model predicted the edge to have curvature in the *x*-direction. Previous work with unsymmetric laminates has not noted this difference between the Rayleigh-Ritz and finite-element predictions of displacement. The lack of a perfectly straight edge has implications in regard to connecting or joining such laminates to other laminates.

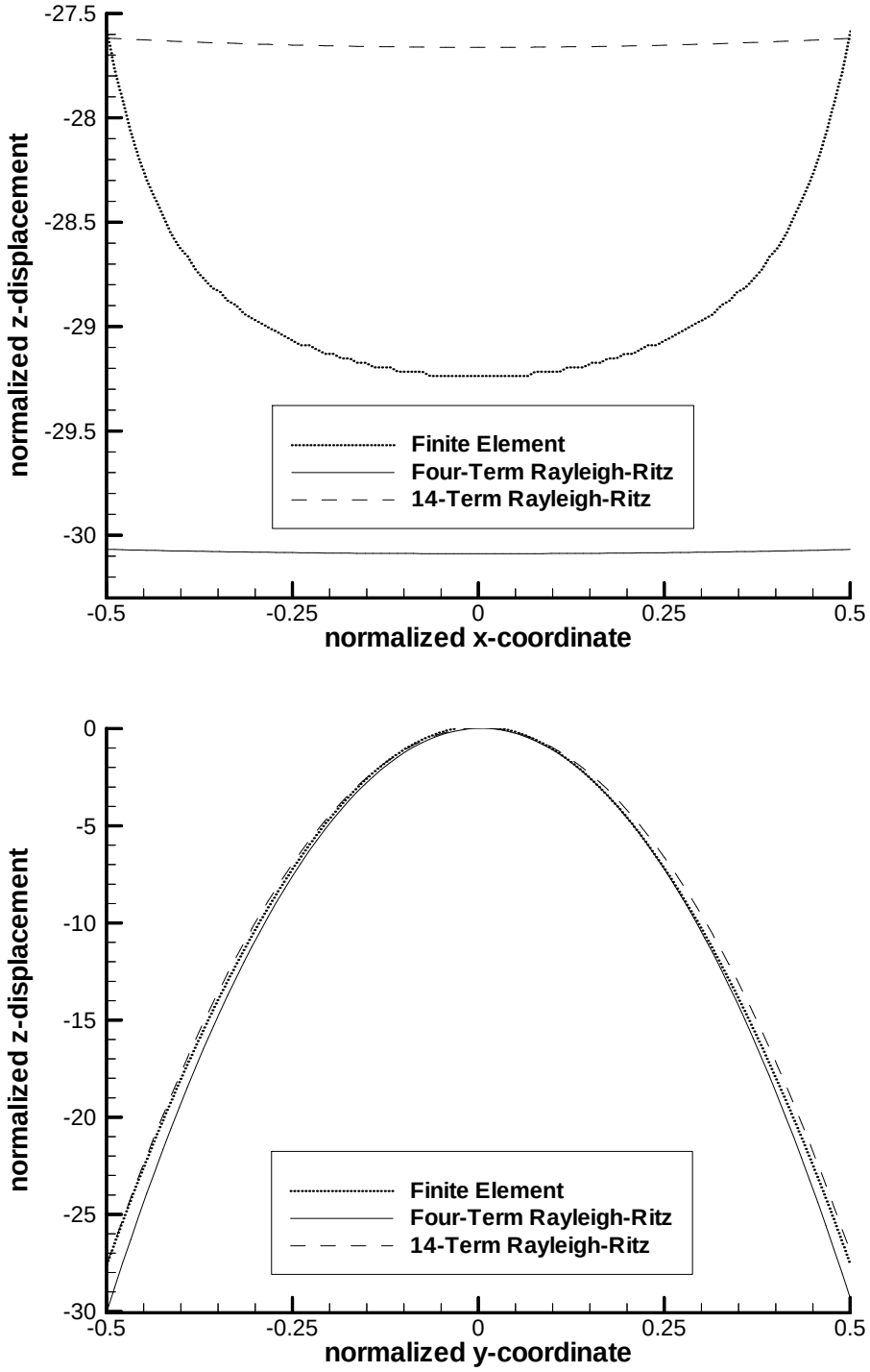

Fig. 3.9 Normalized *z*-displacements along the edges of $[0_4/90_4]_T$ laminate, ΔT=-280°F

Figure 3.10 shows the results for the $[0_6/90_2]_T$ laminate. Once again, the three predictions match the experimental results quite well. Recall from Fig. 3.4 that for a 12 in. side length this laminate is predicted to have but one room-temperature shape.

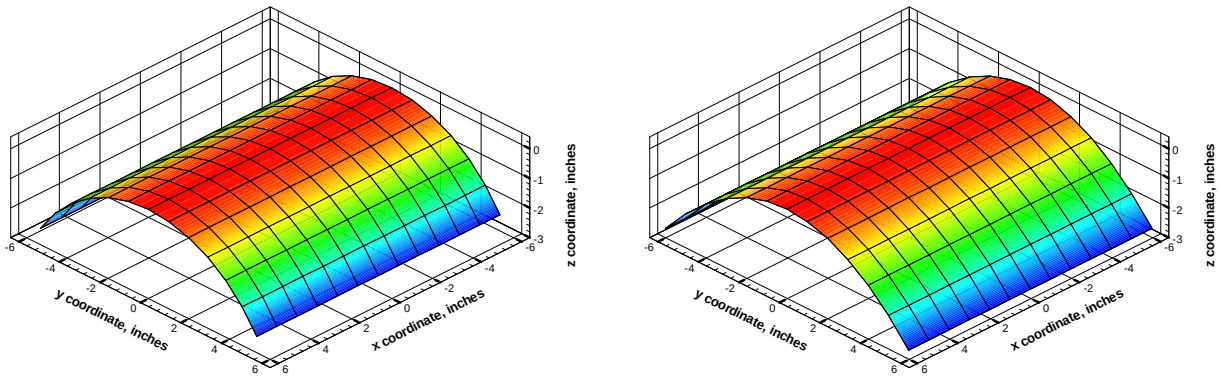

(a) Four-Term Rayleigh-Ritz (b) 14-Term Rayleigh-Ritz

(c) Finite Element (d) Experimental

Fig. 3.10 The primary stable shape of $[0_6/90_2]_T$ laminate, ΔT=-280°F

Figure 3.11 shows the results for the $[0_4/90_2/0_2]_T$ laminate. Again, the three predictions match the experimental results very well. Recall from Fig. 3.5 that there is only stable shape for this 12 in. square laminate at room temperature.

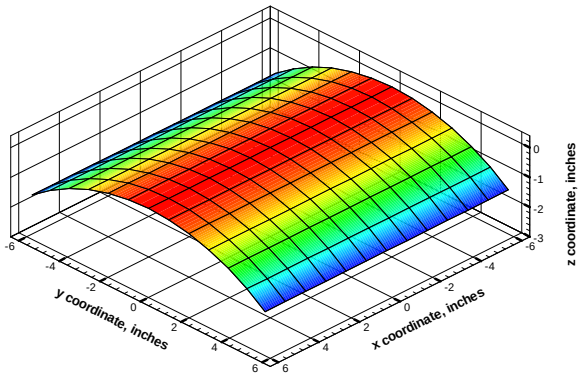

(a) Four-Term Rayleigh-Ritz

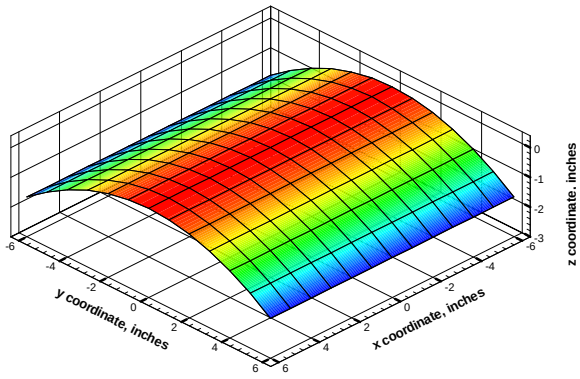

(b) 14-Term Rayleigh-Ritz

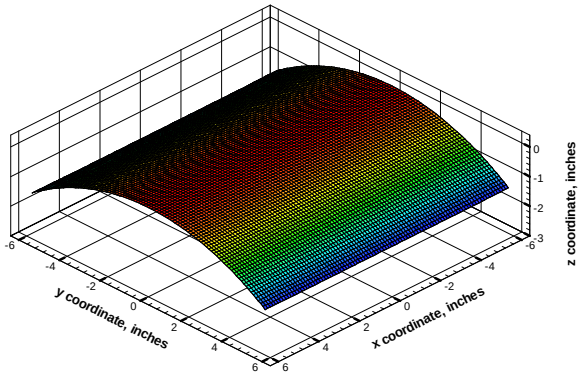

(c) Finite Element

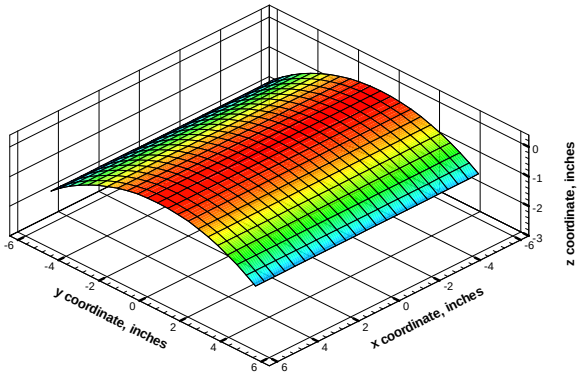

(d) Experimental

Fig. 3.11 The primary stable shape of $[0_4/90_2/0_2]_T$ laminate, ΔT=-280°F

Figure 3.12 shows the primary stable shape for the $[0_2/90_2/0_2/90_2]_T$ laminate. Agreement among the three predictions and the experimental results are good. Although the measured portion of the experimental results, Fig. 3.12(d), suggest a relatively flat shape, the actual panel is curved slightly along the *y*-coordinate. Figure 3.6 shows the existence of an alternate stable shape. This prediction has also been verified by the 14-term Rayleigh-Ritz and finite-element models. The predicted and measured alternate shapes for this laminate are shown in Fig. 3.13. It is important to

note that in this case the finite-element solution has some of the characteristics of a saddle shape, but the Rayleigh-Ritz solutions show less of this tendency.

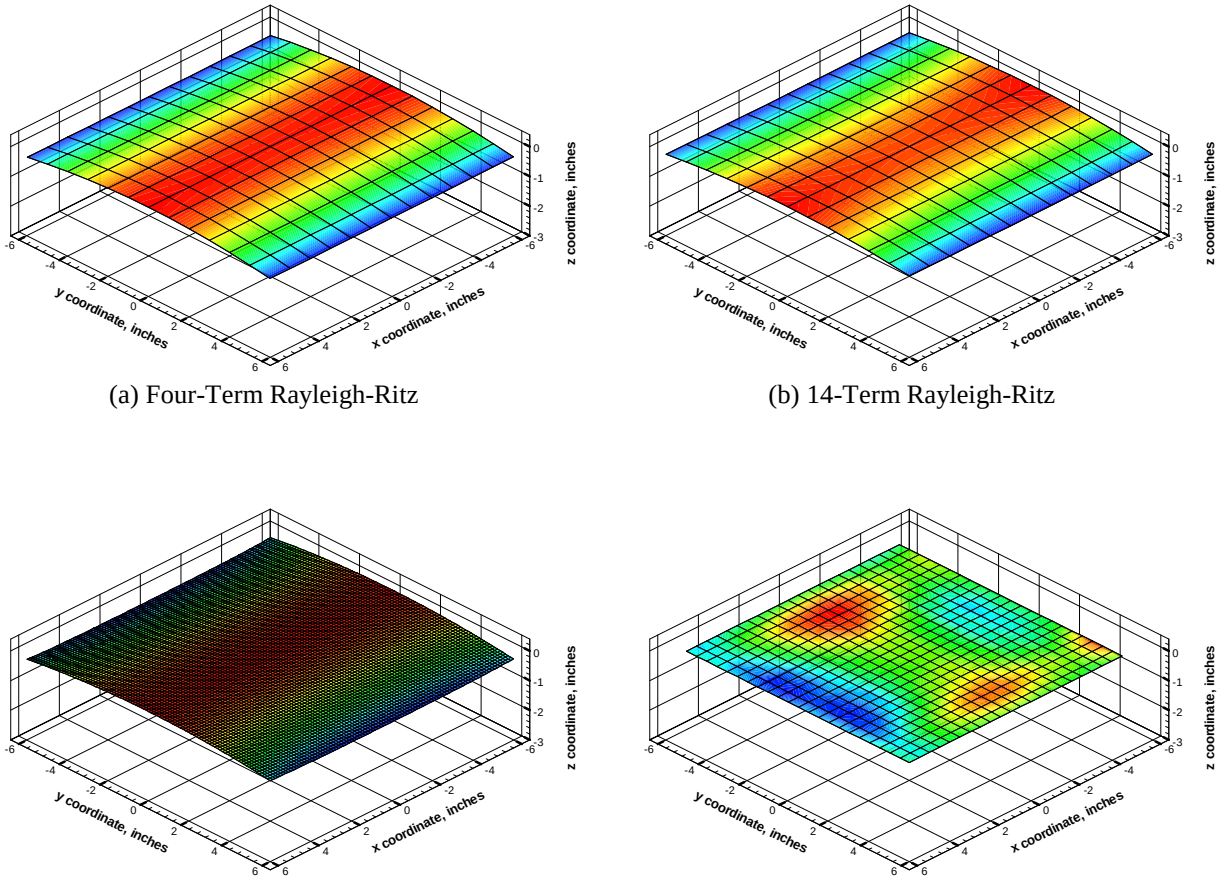

(a) Four-Term Rayleigh-Ritz

(b) 14-Term Rayleigh-Ritz

(c) Finite Element

(d) Experimental

Fig. 3.12 The primary stable shape of $[0_2/90_2/0_2/90_2]_T$ laminate, ΔT=-280°F

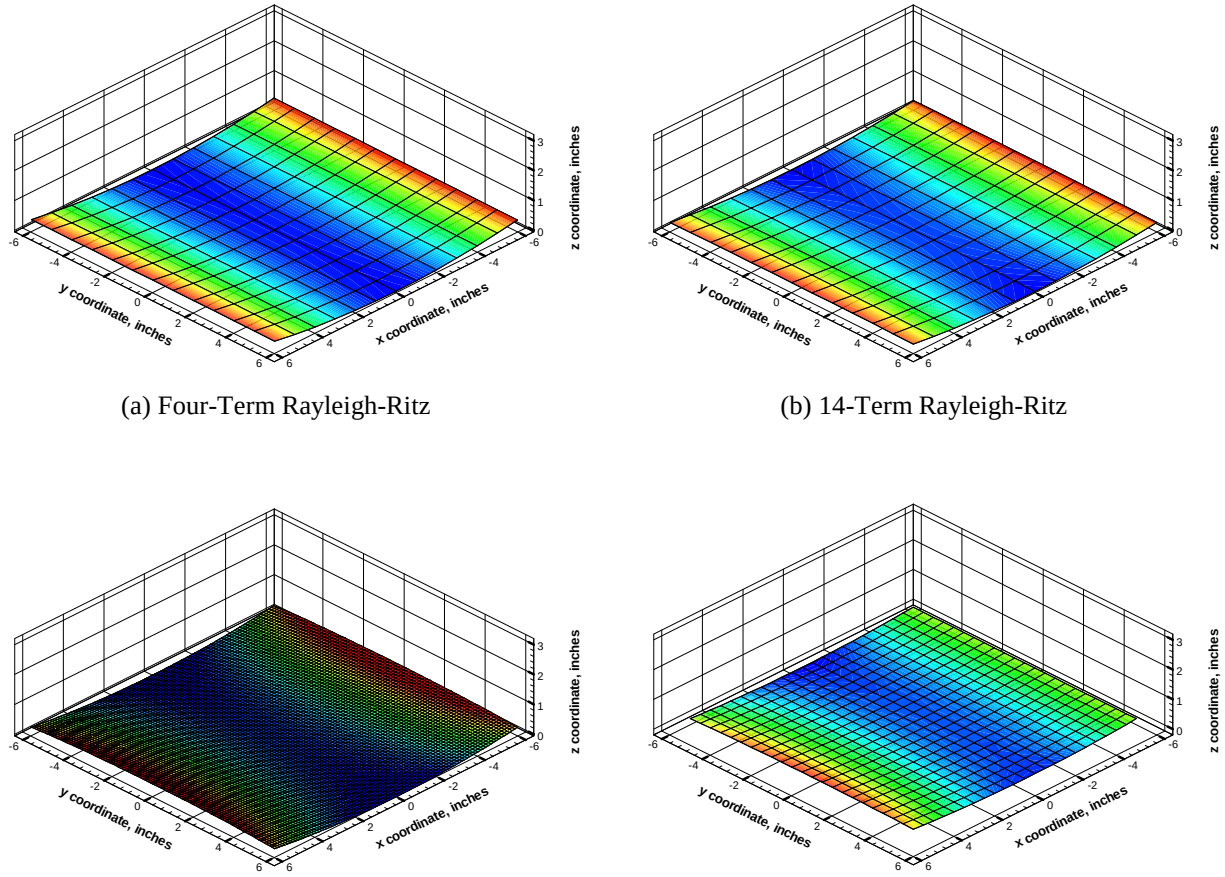

(a) Four-Term Rayleigh-Ritz

(b) 14-Term Rayleigh-Ritz

(c) Finite Element

(d) Experimental

Fig. 3.13 The alternate stable shape of $[0_2/90_2/0_2/90_2]_T$ laminate, ΔT=-280°F

3.3 Angle-ply Laminates

This section focuses on the autoclave-cure-induced deformations of angle-ply laminates. Table 3.2 shows three angle-ply laminates from the $[\theta_2/90/0]_{2T}$ family that will be considered.

Table 3.2 Angle-ply laminate construction

Laminate	**Layup**
Angle-ply 1	$[15_2/90/0]_{2T}$
Angle-ply 2	$[30_2/90/0]_{2T}$
Angle-ply 3	$[45_2/90/0]_{2T}$

These angle-ply laminates are highly unsymmetric, resulting in large deformations that can only be accurately modeled using geometrically nonlinear kinematic theories. In addition, the deformations induced by the off-axis layers lead to complicated shapes that can no longer be approximated by the four-term Rayleigh-Ritz model employed in the previous section. Therefore, two geometrically nonlinear models are used, the 14-term Rayleigh-Ritz model and the finite-element model.

3.3.1 14-Term Rayleigh-Ritz Models

The Rayleigh-Ritz models employs the same approximation of the reference surface strains and curvatures used earlier. The details of the 14-term Rayleigh-Ritz analysis are unchanged from those outlined in Section 3.2.1, and therefore will not be repeated.

3.3.2 Finite-Element Models

The finite-element models are unchanged from the ones used earlier. The details of the model have been outlined in Section 3.2.2, and therefore will not be repeated.

3.3.3 Experimental Measurements

As with the cross-ply laminates, angle-ply specimens were fabricated and the shape measured with a surface profilometer. In addition, the out-of-plane displacement of one of the corners was measured. The results are tabulated in Table 3.3.

3.3.4 Results

Due to its analytical efficiency and its ability to find alternate shapes, the 14-term Rayleigh-Ritz model was used first to compute the curvatures of the 12 in. panels. It was found that this family of angle-ply laminates have only one stable shape. This information was useful because the finite-element computations would be easier than if multiple shapes existed. Figures 3.14-3.16 show the comparison of the predicted deformed shapes with the experimental results of the three laminates at room temperature. For each case, it can be seen that the agreements between predictions and the experimental results are good. Table 3.3 shows the corner displacements of the panels at x=-6 in., y=6 in. These measurements quantify the results of Figs. 3.14-3.16 and show that the displacement measurements were within 15% of the predictions.

Table 3.3 Corner displacements comparison between predicted and measured

Lamination Sequence	Rayleigh-Ritz	Finite Element	Experimental
$[15_2/90/0]_{2T}$	-0.76 in.	-0.79 in.	-0.67 in.
$[30_2/90/0]_{2T}$	-1.22 in.	-1.24 in.	-1.41 in.
$[45_2/90/0]_{2T}$	-1.41 in.	-1.42 in.	-1.51 in.

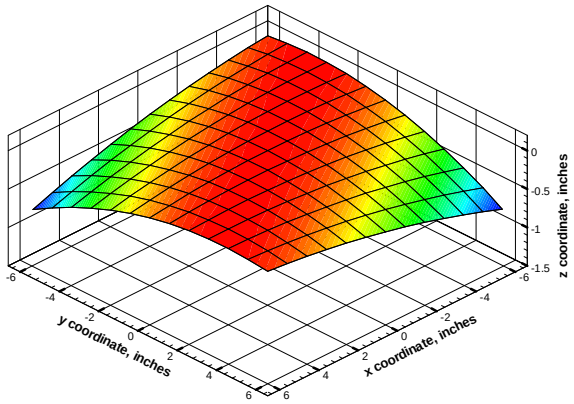

(a) Rayleigh-Ritz $[15_2/90/0]_{2T}$

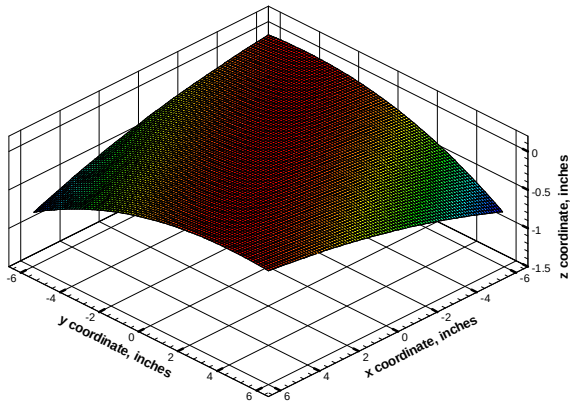

(b) Finite Element $[15_2/90/0]_{2T}$

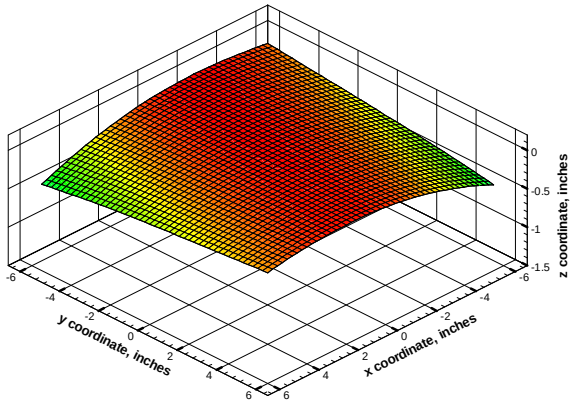

(c) Experimental $[15_2/90/0]_{2T}$

Fig. 3.14 Deformed shape comparison for $[15_2/90/0]_{2T}$ laminate, ΔT=-280°F

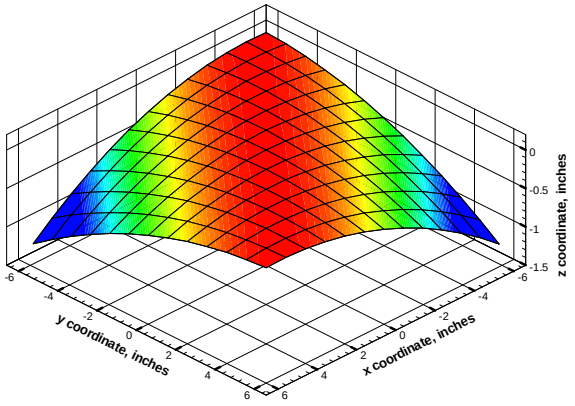

(a) Rayleigh-Ritz $[30_2/90/0]_{2T}$

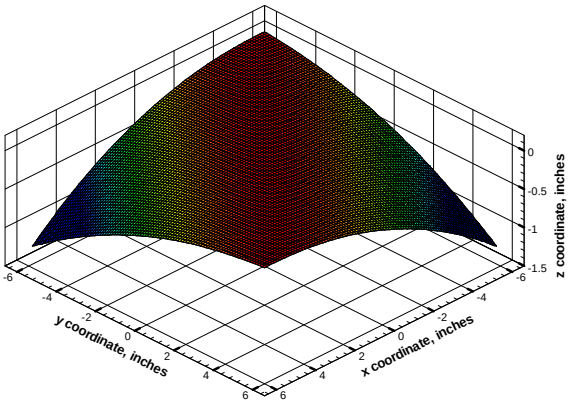

(b) Finite Element $[30_2/90/0]_{2T}$

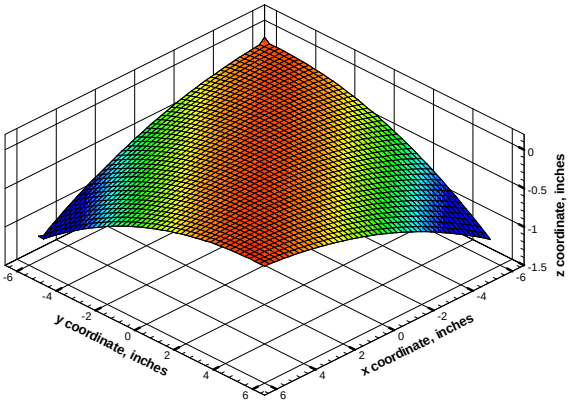

(c) Finite Element $[30_2/90/0]_{2T}$

Fig. 3.15 Deformed shape comparison for $[30_2/90/0]_{2T}$ laminate, ΔT=-280°F

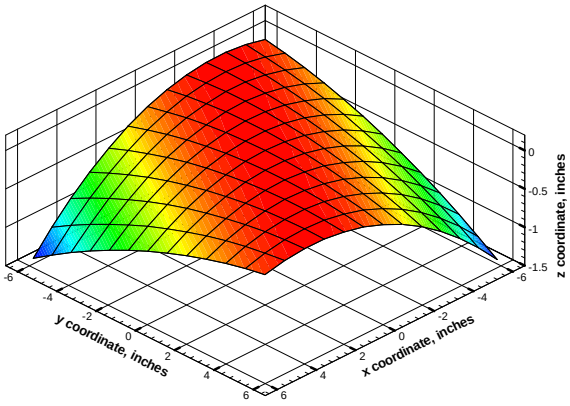

(a) Rayleigh-Ritz $[45_2/90/0]_{2T}$

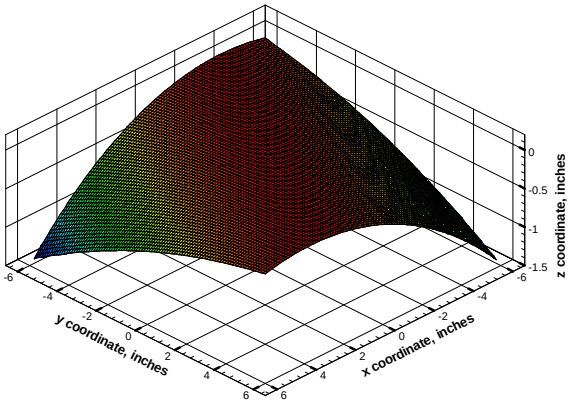

(b) Finite Element $[45_2/90/0]_{2T}$

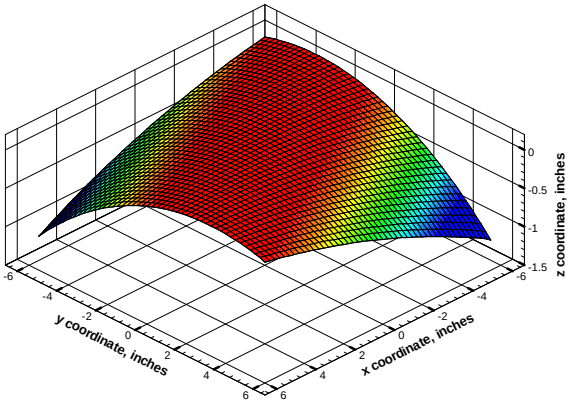

(c) Experimental $[45_2/90/0]_{2T}$

Fig. 3.16 Deformed shape comparison for $[45_2/90/0]_{2T}$ laminate, ΔT=-280°F

3.4 Chapter Conclusions

In Chapter 3 the manufacturing induced deformations of elevated temperature cured unsymmetric composite plates were investigated. The laminates considered were divided into two categories: cross-ply laminates and angle-ply laminates. Four cross-ply laminates were modeled by using four-term Rayleigh-Ritz models, 14-term Rayleigh-Ritz models, and finite-element models. The detailed results of each model were compared, and it was found that the Rayleigh-Ritz models could not capture the details of the edge effects as well as the finite-element models. However, overall agreement among the models was good. Experimental results were obtained by manufacturing actual laminates and measuring the shapes with a mechanical surface profilometer. The correlation between the predictions and the experimental results was found to be good. The $[0_4/90_4]_T$ and $[0_2/90_2/0_2/90_2]_T$ laminates were found to have two stable shapes at room temperature. The existence of an alternate stable shape was successfully predicted by the models, and the shapes agreed well with measurements. Three angle-ply laminates were modeled by using 14-term Rayleigh-Ritz models and finite-element models. The predicted shapes of the laminates by the two models agreed well. All of the angle-ply laminates were found to have only one stable shape. Experimental results were obtained by manufacturing actual specimens and measuring their shapes with a mechanical surface profilometer. The predictions and the experimental results were found to agree well for two of the three laminates.

It was found that the 14-term Rayleigh-Ritz method is the best tool for modeling these laminates. This is because of its analytical efficiency and its ability to find multiple stable configurations, and the fact that the method is based on physical insight. On the average, the Rayleigh-Ritz models required 5% of the processing time required for the finite-element models. This can mean significant reductions in research and development costs. However, the finite-element models can be useful when investigating the details of edge effects that are not captured by the Rayleigh-Ritz models.

Until recently, since curing of graphite/epoxy laminates has always been done at elevated temperature, unsymmetric laminates such as the $[0_4/90_4]_T$ plate considered here are not flat after they are processed. Therefore, there have been few investigations where flat unsymmetric laminates are considered. There may be structural tailoring advantages if an unsymmetric laminate is considered, whereby the coupling between bending and stretching is taken advantage of, but this

issue has never really been addressed. Considering even more basic issues, there have not been many studies of the response of flat unsymmetric laminates to simple loadings. The next chapter begins to examine the response of flat unsymmetric laminates by considering their response to simple inplane compression. The level of inplane compression considered is of such a magnitude that the ensuing out-of-plane deformations are large enough that a geometrically nonlinear analysis is necessary. Additionally, since nonlinear effects are considered, stability is an issue. Therefore in the next chapter, the deformation responses of several flat unsymmetric laminates are considered, and the stability of these responses are examined. Counterpart symmetric laminates are also studied under similar conditions to provide a baseline comparison.